1993

Distance Dependence of Nonadiabaticity in the Branching Between C–Br and C–Cl Bond Fission Following 1[n(O),π*(C=O)] Excitation in Bromopropionyl Chloride

P. W. Kash

G.C.G. Waschewsky

L. J. Butler

Michelle M. Francl
Bryn Mawr College, mfrancl@brynmawr.edu

Custom Citation
P.W. Kash, G.C.G. Waschewsky, L.J. Butler, M.M. Francl. *J. Chem. Phys.* **99** (6), 4479 (1993).

Distance dependence of nonadiabaticity in the branching between C–Br and C–Cl bond fission following $^1[n(O),\pi^*(C{=}O)]$ excitation in bromopropionyl chloride

P. W. Kash, G. C. G. Waschewsky, and L. J. Butler
The James Franck Institute and Department of Chemistry, The University of Chicago, Chicago, Illinois 60637

M. M. Francl
Department of Chemistry, Bryn Mawr College, Bryn Mawr, Pennsylvania 19010

(Received 29 March 1993; accepted 1 June 1993)

These experiments on bromopropionyl chloride investigate a system in which the barrier to C–Br fission on the lowest $^1A''$ potential energy surface is formed from a weakly avoided electronic configuration crossing, so that nonadiabatic recrossing of the barrier to C–Br fission dramatically reduces the branching to C–Br fission. The results, when compared with earlier branching ratio measurements on bromoacetyl chloride, show that the additional intervening CH_2 spacer in bromopropionyl chloride reduces the splitting between the adiabatic potential energy surfaces at the barrier to C–Br fission, further suppressing C–Br fission by over an order of magnitude. The experiment measures the photofragment velocity and angular distributions from the 248 nm photodissociation of $Br(CH_2)_2COCl$, determining the branching ratio between the competing primary C–Br and C–Cl fission pathways and detecting a minor C–C bond fission pathway. While the primary C–Cl:C–Br fission branching ratio is 1:2, the distribution of relative kinetic energies imparted to the C–Br fission fragments show that essentially no C–Br fission results from promoting the molecule to the lowest $^1A''$ potential energy surface via the $^1[n(O),\pi^*(C{=}O)]$ transition; C–Br fission only results from an overlapping electronic transition. The results differ markedly from the predictions of statistical transition state theories which rely on the Born–Oppenheimer approximation. While such models predict that, given comparable preexponential factors, the reaction pathway with the lowest energetic barrier on the $^1A''$ surface, C–Br fission, should dominate, the experimental measurements show C–Cl bond fission dominates by a ratio of C–Cl:C–Br = 1.0: < 0.05 upon excitation of the $^1[n(O),\pi^*(C{=}O)]$ transition. We compare this result to earlier work on bromoacetyl chloride, which evidences a less dramatic reduction in the C–Br fission pathway (C–Cl:C–Br = 1.0:0.4) upon excitation of the same transition. We discuss a model in which increasing the distance between the C–Br and C=O chromophores decreases the electronic configuration interaction matrix elements which mix and split the $^1n(O)\pi^*(C{=}O)$ and $n_p(Br)\sigma^*(C\text{–}Br)$ configurations at the barrier to C–Br bond fission in bromopropionyl chloride. The smaller splitting between the adiabats at the barrier to C–Br fission increases the probability of nonadiabatic recrossing of the barrier, nearly completely suppressing C–Br bond fission in bromopropionyl chloride. Preliminary *ab initio* calculations of the adiabatic barrier heights and the electronic configuration interaction matrix elements which split the adiabats at the barrier to C–Br and C–Cl fission in both bromopropionyl chloride and bromoacetyl chloride support the interpretation of the experimental results. We end by identifying a class of reactions, those allowed by overall electronic symmetry but Woodward–Hoffmann forbidden, in which nonadiabatic recrossing of the reaction barrier should markedly reduce the rate constant, both for ground state and excited state surfaces.

I. INTRODUCTION

This work investigates reactions where the branching ratio between competing bond fission channels is controlled not by the relative heights of the energetic barriers to each bond fission channel, but instead by the relative probability of nonadiabaticity in the transition state region of each bond fission reaction coordinate. In competing bond fission reactions statistical transition state theories[1–3] predict that, given comparable pre-exponential factors, the weakest bond, or the bond with the lowest energetic barrier along the reaction coordinate, will cleave preferentially. These statistical theories successfully predict that the weakest bond in a molecule cleaves preferentially following infrared multiphoton excitation in the ground electronic state.[4,5] However, in photodissociation reactions occurring on excited electronic state surfaces, as well as many bimolecular reactions and concerted unimolecular reactions on ground state surfaces, the barrier along the reaction coordinate often results from an avoided crossing between states of different electronic configurations. The probability of adiabatically crossing these barriers can be dramatically reduced from the rate predicted from statistical theories due to nonadiabatic transitions at the barrier. Consequently, the branching between two different bond fission

channels can be controlled by the relative probability of nonadiabaticity at the barriers to each of the bond fission channels and a bond fission channel with a higher energetic barrier may compete effectively with one with a lower energetic barrier.

In our previous work on the photodissociation of bromoacetyl chloride,[6,7] the results indicated that the competition between C–Cl and C–Br fission upon $^1[n(O),\pi^*(C{=}O)]$ excitation is markedly influenced by nonadiabatic recrossing of the barrier to C–Br fission. On the lowest $^1A''$ excited electronic surface, reached via the $^1[n(O),\pi^*(C{=}O)]$ excitation, the barrier to C–Cl fission is considerably higher than the barrier to C–Br fission, leading to the expectation that C–Br fission would dominate, yet the observed branching was 1.0:0.4 in favor of C–Cl fission. Our model proposed that nonadiabaticity along the C–Br reaction coordinate inhibited crossing of the barrier to C–Br fission, as shown in the left side of Fig. 1. In a simple picture, the barrier along the C–Br reaction coordinate is formed by an avoided electronic crossing between the $^1n(O)\pi^*(C{=}O)$ and the $n_p(Br)\sigma^*(C–Br)$ configurations. To adiabatically cross the barrier to C–Br fission, the electronic wave function must rapidly change from $^1n(O)\pi^*(C{=}O)$ to $n_p(Br)\sigma^*(C–Br)$ character. The experimental branching suggested that the electronic matrix elements between the two configurations were too small for the reaction to proceed over the barrier adiabatically. As a result, when the dynamics sample the barrier to C–Br fission, there is a high probability of retaining the $^1n(O)\pi^*(C{=}O)$ electronic character and then returning into the Franck–Condon region as shown on the left side of Fig. 1. The model further suggests that because the C–Cl bond is alpha to the carbonyl group, the electronic coupling matrix element between the $n_p(Cl)\sigma^*(C–Cl)$ and the $^1n(O)\pi^*(C{=}O)$ configurations is greater than that between the $n_p(Br)\sigma^*(C–Br)$ and the $^1n(O)\pi^*(C{=}O)$ configurations, giving a larger splitting between the adiabats at the saddle point along the reaction coordinate leading to C–Cl fission (Fig. 1, right) than at the barrier to C–Br fission. This results in a higher probability of crossing the barrier to C–Cl fission adiabatically and, consequently, preferential C–Cl bond fission.

The work described here further elucidates how the intramolecular electronic coupling matrix elements, which, when too small, allow nonadiabatic barrier recrossing, depend on the distance and relative orientation between the orbitals involved in the configuration crossing. Here we experimentally determine the C–Cl:C–Br bond fission ratio after a $^1[n(O),\pi^*(C{=}O)]$ transition in bromopropionyl chloride, where we have effectively increased the distance between the orbitals on the C–Br and C=O chromophores. If the electronic coupling matrix elements between the $n_p(Br)\sigma^*(C–Br)$ and $^1n(O)\pi^*(C{=}O)$ configurations decrease strongly with the increased distance between the two chromophores, we should observe a marked increase in nonadiabaticity, resulting in a decrease in the branching to the C–Br bond fission channel in comparison with C–Br fission in bromoacetyl chloride. We present crossed laser-molecular beam measurements of the

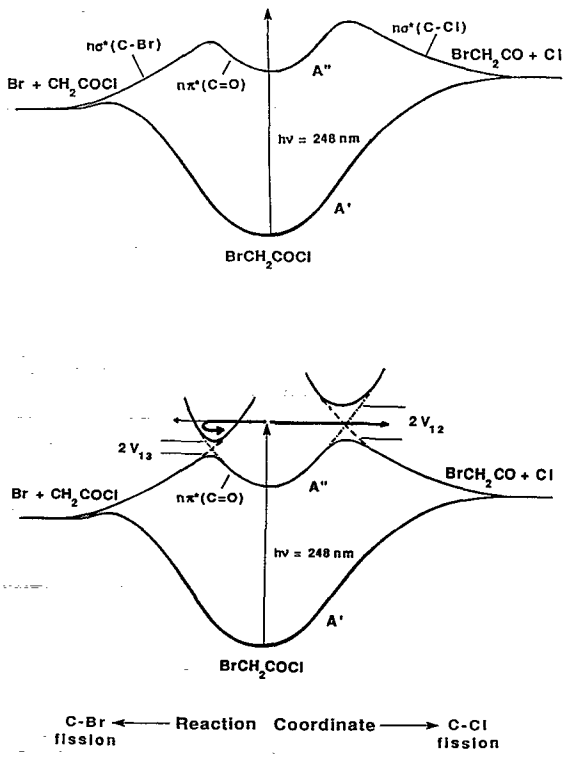

FIG. 1. Schematic reaction coordinates for C–Cl and C–Br bond fission from the 248 nm photodissociation of bromoacetyl chloride. The upper frame shows only the lowest $^1A''$ adiabatic excited electronic surface where the barrier to C–Br bond fission is lower than the barrier to C–Cl bond fission. Considering only this lowest adiabat leads to the incorrect prediction that C–Br bond fission should dominate in bromoacetyl chloride. The lower frame shows this lowest $^1A''$ adiabat along with the upper $^1A''$ adiabats which are formed from the avoided electronic configuration crossing at the barriers to C–Cl and C–Br bond fission. In addition, the dotted lines in the lower frame show the diabatic electronic states. Preferential C–Cl bond fission in bromoacetyl chloride results because the greater coupling V_{12} between the $n(O)\pi^*(C{=}O)$ and the $n(Cl)\sigma^*(C–Cl)$ states allows the molecules to switch from one configuration to the other, resulting in adiabatic crossing of the barrier to C–Cl bond fission. The smaller coupling V_{13} between the $n(O)\pi^*(C{=}O)$ and the $n(Br)\sigma^*(C–Br)$ states results in trajectories retaining the $n(O)\pi^*(C{=}O)$ configuration by making a nonadiabatic hop at the avoided crossing which forms the barrier to C–Br fission, so more trajectories turn back from the repulsive wall on the $n(O)\pi^*(C{=}O)$ surface, reducing the branching to C–Br fission.

branching ratios between the primary photodissociation channels and the velocity and angular distributions of the photofragments to compare the dissociation mechanism of bromopropionyl chloride with our earlier study of bromoacetyl chloride. To complement the experimental results, we present *ab initio* electronic structure calculations of the potential energy surfaces and important electronic coupling matrix elements in these systems. The results not only emphasize the need to consider the intramolecular electronic coupling necessary to adiabatically cross the barrier to each bond dissociation channel, but also provide insight into the factors which control these couplings.

II. EXPERIMENTAL METHOD

To measure the photofragment velocities and angular distributions from the photodissociation of bromopropio-

nyl chloride, $BrCH_2CH_2COCl$, we use a crossed laser-molecular beam apparatus.[8,9] Upon photodissociation with a pulsed excimer laser, neutral dissociation products scatter from the crossing point of the laser and the molecular beam with velocities determined by the vector sum of the molecular beam velocity and the recoil velocity imparted in the dissociation. Those scattered into the acceptance angle of the differentially pumped detector travel 44.1 cm to an electron bombardment ionizer and are ionized by 200 eV electrons. After mass selection with a quadrupole mass filter, the ions are counted with a Daly detector and multichannel scaler with respect to their time-of-flight (TOF) from the interaction region after the dissociating laser pulse. Upon subtraction of the calibrated ion flight time, forward convolution fitting of the TOF spectrum determines the distribution of energies released to relative product translation in the dissociation. The angular distribution of the scattered photofragments is obtained with a linearly polarized photolysis beam by measuring the variation in signal intensity with the direction of the electric vector of the laser in the molecular beam/detector scattering plane.

The molecular beam was formed by expanding gaseous bromopropionyl chloride (at its vapor pressure at 50 °C) seeded in He to give a total stagnation pressure of 300 Torr. The 0.076 mm diameter nozzle was heated to 100 °C to prevent clustering of parent molecules during expansion. The peak beam velocity was 1.28×10^5 cm/s with a full-width-at-half-maximum of 11.5%. To measure the velocity of the parent molecular beam *in situ*, the molecular beam source was rotated to point into the detector and a chopper wheel raised into the beam. To measure the velocities of the neutral photofragments, the molecular beam source is rotated to a different angle in the plane containing the beam and detector axis, a plane perpendicular to the laser beam propagation direction. Laser polarization angles and molecular beam source angles are given here with respect to the detector axis, one defined as positive with clockwise rotation and the other as positive with counterclockwise rotation.

Time-of-flight and angular distribution measurements were made on bromopropionyl chloride photofragments at 248 nm with the source angle maintained at 10° with respect to the detector axis. The unpolarized laser power from a Questek 2640 excimer was typically 175 mJ/pulse with the light focused to a 5 mm^2 spot size at the crossing region of the laser and molecular beam. Polarized spectra typically were taken at 30 mJ/pulse and the same soft focus. Quadrupole resolution was adjusted to 1.2 amu FWHM for $m/e^+=35$ (Cl^+) and for $m/e^+=79$ (Br^+) for all data on bromopropionyl chloride. For the anisotropy measurements, we dispersed the unpolarized laser light into two linearly polarized components with a single crystal quartz Pellin–Broca and used the horizontal component, rotating the polarization into the desired direction with a half-wave retarder. The polarization dependent signal, integrated in many repeated short scans and alternating between each laser polarization direction, required no additional normalization to laser power or detector efficiency.

The only detectable signal which results from parent bromopropionyl chloride photodissociation at 248 nm came from Br^+, Cl^+, and $C_2H_2^+$. All observed signal could be fit with three competing dissociation channels, C–C, C–Br, and C–Cl fission. Although signal was detected at $CH_2CH_2COCl^+$, $BrCH_2CH_2CO^+$, $COCl^+$, $BrCH_2CH_2^+$, and $BrCH_2^+$, the nearly identical slow arrival times for all of these fragments indicate that they result from dissociation of clusters in the molecular beam. No significant signal was seen above the background at the masses corresponding to CH_3^+ after 100 000 shots, CH_2COCl^+ after 250 000 shots, $CH_2CH_2CO^+$ after 300 000 shots, or CH_2CO^+ after 300 000 shots. Nor was signal from molecular elimination products detected at HCl^+, $BrCl^+$, or HBr^+ after over 300 000 shots each.

III. COMPUTATIONAL METHOD

To support and facilitate interpretation of the experimental results, we also present *ab initio* electronic structure calculations for bromopropionyl chloride using the GAUSSIAN 92 system of programs[10] with a STO-3G* basis set. Configuration interaction with single and double excitations (CISD) calculations provide electronic ground state energies in the harmonic region of the C–Cl, C–Br, and C=O stretching potentials. These energies in the harmonic region are then fit to a Morse oscillator with the correct dissociation energy. The ground state energy, as a function of the C–Cl, C–Br, and C=O stretching coordinates, is then assumed to be a sum of three independent Morse oscillators. Configuration interaction with single excitations (CIS) calculations provide excitation energies from the ground electronic state to the relevant excited electronic states. These CIS excitation energies are added to the ground state Morse oscillator energies to construct the excited electronic state surfaces. Calculation of the excited electronic states provides the relative barrier heights to C–Br and C–Cl bond fission along the lowest adiabatic $^1A''$ excited electronic state. In addition, the calculations also provide energetic splittings between the two lowest adiabatic $^1A''$ excited electronic states at the avoided crossing in both the C–Cl and C–Br bond fission channels.

Because the $^1n(O)\pi^*(C{=}O)$ $^1A''$ excited electronic state, accessed by a 248 nm photon, has a longer equilibrium C=O bond distance than in the ground electronic state, we present CIS calculations of the avoided crossing region on the excited $^1A''$ electronic surfaces at a variety of C=O bond distances which represent the range of C=O stretching motion likely sampled by the dissociative wave function. In addition, to compare the present experimental and theoretical results for bromopropionyl chloride with our previous results for bromoacetyl chloride, we also present *ab initio* CIS and CISD calculations on bromoacetyl chloride.

IV. RESULTS AND ANALYSIS

A. Overview

The data below examines the branching between primary C–Cl and C–Br bond fission in bromopropionyl chlo-

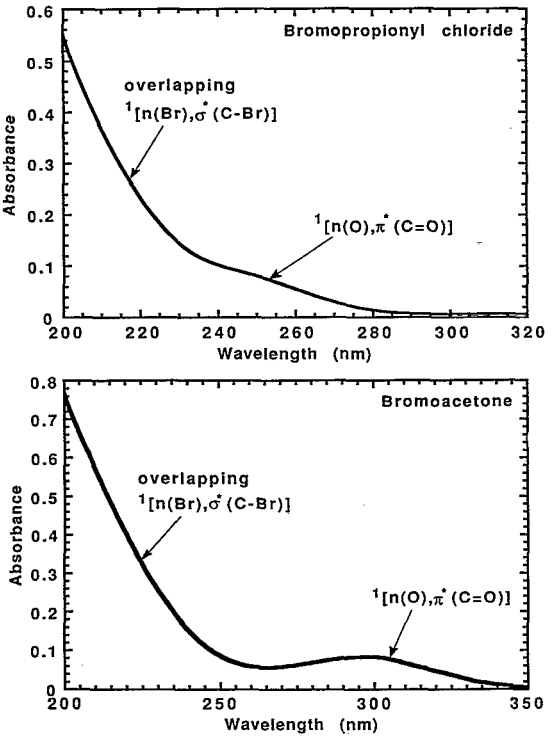

FIG. 2. Ultraviolet absorption spectra of bromopropionyl chloride (upper frame) and bromoacetone (lower frame). In bromopropionyl chloride the lower energy $n(O)\rightarrow\pi^*(C{=}O)$ transition, peaking near 255 nm, is clearly seen as a shoulder on the higher energy $n_p(Br)\rightarrow\sigma^*(C\text{-}Br)$ transition. In bromoacetone the same $n(O)\rightarrow\pi^*(C{=}O)$ transition is red shifted, peaking near 300 nm, and is clearly separated from the higher energy $n_p(Br)\rightarrow\sigma^*(C\text{-}Br)$ transition. The spectra were recorded on a Perkin–Elmer Lambda 6 UV/VIS spectrophotometer at each sample's equilibrium vapor pressure at room temperature (1 cm path length).

ride upon excitation at 248 nm, which is in an overlapping region of the strong $[n_p(Br),\sigma^*(C\text{-}Br)]$ and $^1[n(O),\pi^*(C{=}O)]$ transitions (see Fig. 2), and compares the findings with our previous results on bromoacetyl chloride photodissociation at 248 nm. The experimental results and analysis in Sec. IV B address the competition between C–Cl alpha bond cleavage and fission of the weaker C–Br bond in bromopropionyl chloride. C–Br bond fission in bromopropionyl chloride at 248 nm can result from both of the overlapping electronic transitions. To separate these two contributions, we compare the C–Br fission in bromopropionyl chloride with C–Br fission in bromoacetyl chloride at 248 nm, where C–Br bond cleavage also results from both of the overlapping $[n_p(Br),\sigma^*(C\text{-}Br)]$ and $^1[n(O),\pi^*(C{=}O)]$ transitions, and with C–Br fission in bromoacetone at 308 nm, where C–Br fission results only from the $^1[n(O),\pi^*(C{=}O)]$ transition. The results show that following an $^1[n(O),\pi^*(C{=}O)]$ transition C–Br bond fission in bromopropionyl chloride is reduced by at least a factor of 10 in comparison with bromoacetyl chloride.

Section IV C presents the results of *ab initio* calculations of the excited electronic states involved in the 248 nm photodissociation dynamics of both bromoacetyl and bromopropionyl chloride. The results show that in both molecules, on the lowest $^1A''$ adiabatic excited electronic state, the barrier to C–Cl bond fission is approximately 10 kcal/mol higher than the barrier to C–Br bond fission, resulting in an incorrect prediction of preferential C–Br bond fission when considering only this single adiabatic Born–Oppenheimer surface. However, the *ab initio* calculations also show that the splitting between adiabats at the barrier to C–Cl bond fission is significantly greater than the splitting between adiabats at the barrier to C–Br bond fission, suggesting that the experimentally observed preferential C–Cl bond fission in both molecules results from suppression of C–Br bond fission due to nonadiabatic recrossing of the barrier to C–Br bond fission. The calculations also show that the factor of 10 decrease in C–Br bond fission in bromopropionyl chloride vs bromoacetyl chloride results because the splitting between adiabats at the barrier to C–Br bond fission is approximately ten times smaller in bromopropionyl chloride than in bromoacetyl chloride. In the discussion we show that this smaller splitting between adiabats at the barrier to C–Br bond fission in bromopropionyl chloride results because increasing the distance between the C=O and C–Br chromophores decreases the electronic configuration interaction matrix elements between the $^1n(O)\pi^*(C{=}O)$ and $n_p(Br)\sigma^*(C\text{-}Br)$ configurations which mix and split to form the barrier to C–Br bond fission.

B. Preferential fission of the C–Cl alpha bond over the C–Br bond in bromopropionyl chloride

1. Determination of primary photofragmentation channels

Figure 3 shows the TOF spectra of the primary photofragments of $BrCH_2CH_2COCl$ excited at 248 nm. All of the signal can be fit to three competing dissociation channels, fission of the C–Br bond, fission of the C–Cl bond α to the carbonyl, and fission of the C–C bond α to the carbonyl:

$$BrCH_2CH_2COCl + h\nu(248\ \text{nm}) \rightarrow Br + CH_2CH_2COCl, \quad (1)$$

$$BrCH_2CH_2COCl + h\nu(248\ \text{nm}) \rightarrow BrCH_2CH_2CO + Cl, \quad (2)$$

$$BrCH_2CH_2COCl + h\nu(248\ \text{nm}) \rightarrow BrCH_2CH_2 + COCl. \quad (3)$$

The fast portion of the Br^+ signal, peaking near 240 μs, results from primary C–Br fission and is fit with the translational energy distribution shown in Fig. 4. The momentum matched partner CH_2CH_2COCl fragment cracks to Cl^+ in the ionizer and results in the small signal arriving near 260 μs in the Cl^+ spectra. As expected, since the CH_2CH_2COCl fragment has a slightly larger mass than the Br fragment, the Cl^+ daughter ions from the CH_2CH_2COCl fragment arrive at the detector slightly later than the momentum matched Br partner. The fast portion of the Cl^+ signal, peaking near 200 μs, results from primary C–Cl fission and is fit with the translational energy

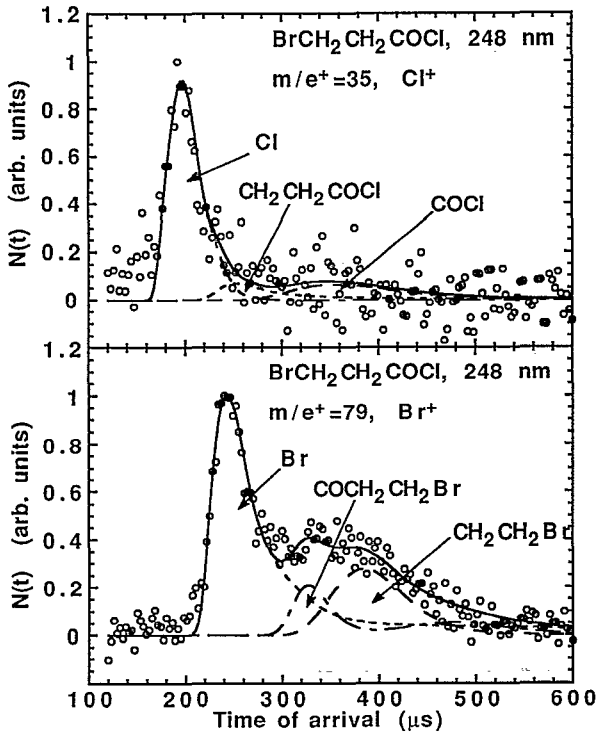

FIG. 3. Laboratory time-of-flight spectra of the photofragments of bromopropionyl chloride detected at Cl^+ (upper frame) and Br^+ (lower frame) at 248 nm with an unpolarized laser. Signals in the upper and lower frames were integrated for 1 000 000 and 250 000 laser shots, respectively. The source angle was 20° in the upper frame and 10° in the lower frame. The contribution from $ClCOCH_2CH_2$ fragments to the Cl^+ spectrum was determined by fitting the signal with the $P(E_T)$ derived from forward convolution fitting the fastest portion of the Br^+ signal which results from primary C–Br bond fission. Similarly, the contribution from $COCH_2CH_2Br$ fragments to the Br^+ spectrum was determined by fitting the signal with the $P(E_T)$ derived from forward convolution fitting the fastest portion of the Cl^+ signal which results from primary C–Cl bond fission. The contribution from ClCO fragments to the Cl^+ spectrum and from CH_2CH_2Br fragments to the Br^+ spectrum was determined by fitting the respective signals with the $P(E_T)$ derived from forward convolution fitting the slowest portion of the CH_3CO^+ signal in the 308 nm photodissociation of bromoacetone (Ref. 12).

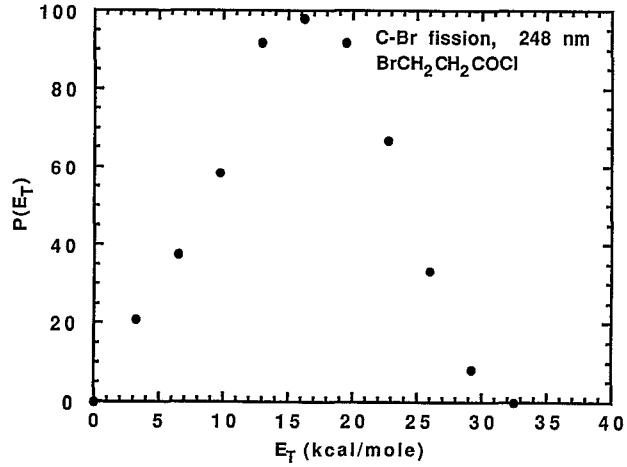

FIG. 4. The center-of-mass product translational energy distribution, $P(E_T)$, for the C–Br fission channel in bromopropionyl chloride at 248 nm. The $P(E_T)$ is derived from forward convolution fitting the fastest component of the Br^+ signal in the lower frame of Fig. 3 and is used to fit the contribution from $ClCOCH_2CH_2$ in the Cl^+ signal in the upper frame of Fig. 3. This Gaussian-shaped $P(E_T)$ results almost entirely from the $n_p(Br) \rightarrow \sigma^*(C\text{–}Br)$ transition with minimal or no contribution from the overlapping $n(O) \rightarrow \pi^*(C{=}O)$ transition.

distribution shown in Fig. 5 (upper frame). The similarity between the translational energy distribution for C–Cl fission in bromopropionyl chloride with the translational energy distribution previously reported for C–Cl fission following 248 nm photolysis of bromoacetyl chloride[7] (Fig. 5 lower frame) and acetyl chloride[11] supports the assignment of this fast portion of the signal as resulting from primary C–Cl fission. In addition, the $BrCH_2CH_2CO$ partner in C–Cl fission cracks to the Br^+ daughter ion and results in the contribution to the slow shoulder in the Br^+ spectra peaking near 320 μs. Finally, after considering only C–Br and C–Cl fission, it was impossible to fit the slow broad tail in the Br^+ spectra and the slow small signal near 350 μs in the Cl^+ spectra. However, assuming some primary C–C α bond fission was occurring and assuming the same translational energy distribution for C–C fission as obtained in the 308 nm photodisociation of bromoacetone[12] (Fig. 6), we obtained a nearly perfect fit of the slowest Br^+ and Cl^+ signal. Consequently, while we can not detect either of the primary photofragments from C–C bond fission at the parent ion, the primary $BrCH_2CH_2$ and COCl fragments must crack to Br^+ and Cl^+ in the ionizer, resulting in observed contributions to the Br^+ and Cl^+ spectra at slow arrival times.

2. Identifying the C–Br fission due to $^1[n(O),\pi^*(C{=}O)]$ excitation and the overlapping $[n(Br),\sigma^*(C\text{–}Br)]$ transition

The absorption spectrum of bromopropionyl chloride (Fig. 2 upper frame), like that of bromoacetyl chloride,[7] clearly indicates that at 248 nm the $^1[n(O),\pi^*(C{=}O)]$ transition overlaps with the higher energy $[n_p(Br), \sigma^*(C\text{–}Br)]$ transition. Since the $[n_p(Br),\sigma^*(C\text{–}Br)]$ transition promotes the molecule to an electronic state repulsive in the C–Br bond, the observed C–Br fission may result from a combination of direct dissociation on this repulsive surface and dissociation via the $^1[n(O),\pi^*(C{=}O)]$ transition. To separate these two possible contributions to C–Br fission, we analyze the shape of the distribution of kinetic energies for C–Br fission at 248 nm with respect to that for dissociation via the $^1[n(O),\pi^*(C{=}O)]$ excitation alone and with respect to the distribution expected for direct dissociation on the $n_p(Br)\sigma^*(C\text{–}Br)$ repulsive electronic surface. {The observed C–Cl and C–C fission clearly results from the $^1[n(O),\pi^*(C{=}O)]$ excitation. Both the $[n_p(Cl),\sigma^*(C\text{–}Cl)]$ transition and the transition to the $\sigma\sigma^*(C\text{–}C)$ surface occur at much higher energies. In addition, the $P(E_T)$ for C–Cl fission is nearly identical to that for acetyl chloride and bromoacetyl chloride where the C–Cl fission has been previously shown to result from the $^1[n(O),\pi^*(C{=}O)]$ transition. Similarly, since the $P(E_T)$ for C–C fission is identical to that in bromoacetone[12] excited at the 308 nm

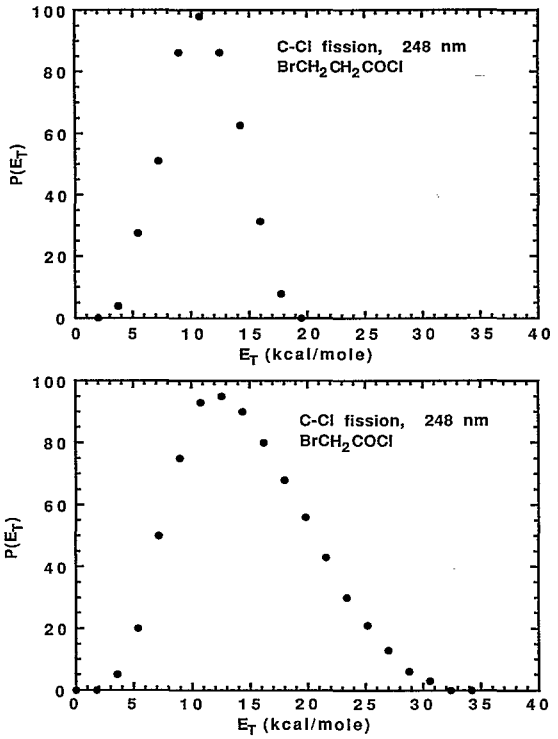

FIG. 5. The center-of-mass product translational energy distribution, $P(E_T)$, for the C–Cl fission channel in bromopropionyl chloride (upper frame) and bromoacetyl chloride (lower frame) at 248 nm. The $P(E_T)$ in the upper frame is derived from forward convolution fitting the fastest component of the Cl^+ signal, from the 248 nm photodissociation of bromopropionyl chloride, in the upper frame of Fig. 3 and is used to fit the contribution from $COCH_2CH_2Br$ to the Br^+ signal in the lower frame of Fig. 3. The similarity in the $P(E_T)$'s for C–Cl fission in bromopropionyl and bromoacetyl chloride suggest that all of the C–Cl fission in bromopropionyl chloride results from the from the same $n(O)\pi^*(C{=}O)$ transition previously shown to produce C–Cl fission in bromoacetyl chloride.

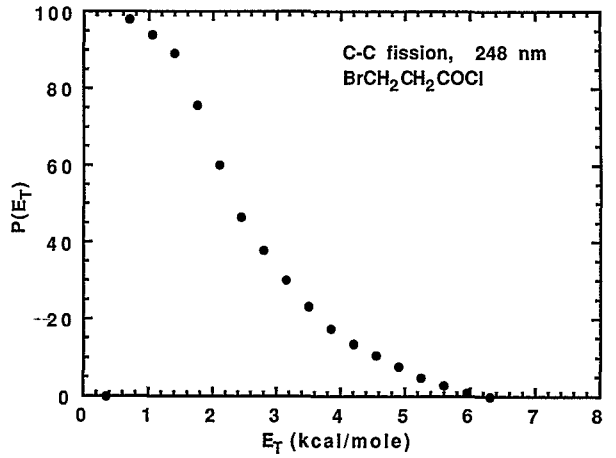

FIG. 6. The center-of-mass product translational energy distribution, $P(E_T)$, for the C–C fission channel in bromoacetone at 308 nm (Ref. 12). The $P(E_T)$ is derived from forward convolution fitting the CH_3CO^+ signal (not shown here) which results from primary C–C bond fission. This $P(E_T)$ is used to fit the contribution from ClCO to the Cl^+ signal resulting from the 248 nm photodissociation of bromopropionyl chloride in the upper frame of Fig. 3 and the contribution from CH_2CH_2Br to the Br^+ signal from the 248 nm photodissociation of bromopropionyl chloride in the lower frame of Fig. 3.

$^1[n(O),\pi^*(C{=}O)]$ transition, all C–C fission in bromopropionyl chloride also results from the $^1[n(O),\pi^*(C{=}O)]$ transition.}

To identify the relative contribution of each electronic transition to the observed signal from C–Br bond fission in bromopropionyl chloride, we first review the translational energy distribution for C–Br bond fission in bromoacetyl chloride[7] to determine the shape of the $P(E_T)$ characteristic of C–Br fission resulting from $^1[n(O),\pi^*(C{=}O)]$ excitation and the shape of the $P(E_T)$ characteristic of C–Br fission resulting from the overlapping $[n_p(Br),\sigma^*(C\text{–}Br)]$ excitation. Figure 7 shows the $P(E_T)$ for C–Br fission in bromoacetyl chloride photodissociated at 248 nm. [Note that this $P(E_T)$ has slightly less probability at small translational energies than the $P(E_T)$ we previously reported for C–Br bond fission in bromoacetyl chloride. In our forthcoming work on bromoacetone[12] photodissociation at 308 nm, we show that the slow portion of the Br^+ signal from the 248 nm photodissociation of bromoacetyl chloride actually results from primary C–C bond fission instead of the previously assigned C–Br bond fission.] Since the 248 nm excitation of bromoacetyl chloride is, like bromopropionyl chloride, in a region of the absorption spectra where the $^1[n(O),\pi^*(C{=}O)]$ and $[n_p(Br),\sigma^*(C\text{–}Br)]$ transitions overlap, the $P(E_T)$ for C–Br fission in Fig. 7 can result from contributions from both of these overlapping electronic transitions. The $^1[n(O),\pi^*(C{=}O)]$ transition in bromoacetone, however, is shifted to much lower energies (Fig. 2 lower frame) and the $^1[n(O),\pi^*(C{=}O)]$ and $[n_p(Br),\sigma^*(C\text{–}Br)]$ transitions are well separated. Excitation of bromoacetone at 308 nm, then, necessarily excites only the $^1[n(O),\pi^*(C{=}O)]$ electronic transition.

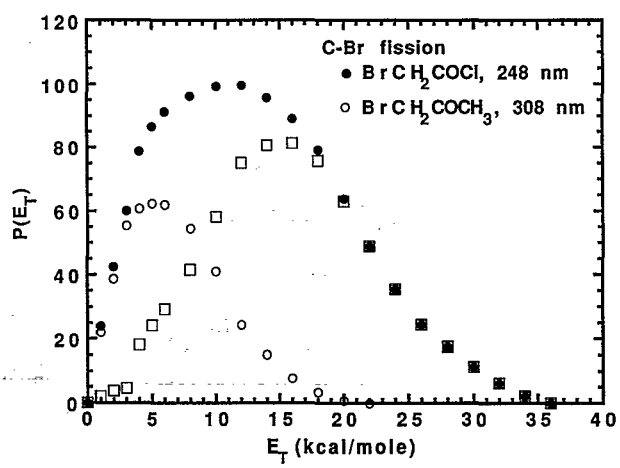

FIG. 7. The center-of-mass product translational energy distribution, $P(E_T)$, for the C–Br fission channel in bromoacetyl chloride at 248 nm (closed circles) overlaid with the $P(E_T)$ for C–Br fission in bromoacetone at 308 nm (open circles). All of the C–Br fission in bromoacetone results from the $n(O)\pi^*(C{=}O)$ transition so the lower energy portion of the bromoacetyl chloride $P(E_T)$ is also attributed to C–Br fission resulting from the $n(O)\pi^*(C{=}O)$ transition. The squares, which are the result of subtracting the bromoacetone $P(E_T)$ from the bromoacetyl chloride $P(E_T)$, represent the $P(E_T)$ for C–Br bond fission in bromoacetyl chloride resulting only from the overlapping $n_p(Br)\sigma^*(C\text{–}Br)$ transition.

Consequently, the $P(E_T)$ for primary C–Br bond fission in the 308 nm photodissociation of bromoacetone,[12] shown in Fig. 7, represents the distribution which results only from the $^1[n(O),\pi^*(C{=}O)]$ transition. As Fig. 7 shows, this $P(E_T)$ for C–Br fission in bromoacetone overlaps well with the low energy portion of the $P(E_T)$ for C–Br fission in bromoacetyl chloride, suggesting that this low energy portion of the bromoacetyl chloride $P(E_T)$ also results from the $^1[n(O),\pi^*(C{=}O)]$ transition. The higher energy portion of the bromoacetyl chloride $P(E_T)$, not well matched by the bromoacetone $P(E_T)$, must then result from the overlapping $[n_p(Br),\sigma^*(C–Br)]$ transition in bromoacetyl chloride. To determine the shape of the $P(E_T)$ representative of C–Br fission resulting from the overlapping $[n_p(Br),\sigma^*(C–Br)]$ excitation, we subtract this bromoacetone $P(E_T)$, which results only from the $^1[n(O),\pi^*(C{=}O)]$ transition, from the bromoacetyl chloride $P(E_T)$, which results from a combination of the overlapping $^1[n(O),\pi^*(C{=}O)]$ and $[n_p(Br),\sigma^*(C–Br)]$ transitions. This subtracted $P(E_T)$ for C–Br fission from the overlapping transition is shown with square symbols in Fig. 7 and compared to that from brompropionyl chloride in the next paragraph. (We should note that, first, this separation into two components is only approximate and, further, it is based on the classical assumption that any interference between the two pathways is negligible.)

With the separate translational energy distributions characteristic of C–Br fission resulting from an $^1[n(O),\pi^*(C{=}O)]$ and an $[n_p(Br),\sigma^*(C–Br)]$ transition, obtained in the deconvolution of the bromoacetyl chloride $P(E_T)$ above, we can now determine which electronic transition contributes to the observed C–Br bond fission in bromopropionyl chloride. As stated above, excitation of bromopropionyl chloride at 248 nm also accesses a portion of the absorption spectrum where the $^1[n(O),\pi^*(C{=}O)]$ transition is overlapped by an $[n_p(Br),\sigma^*(C–Br)]$ transition. Consequently, the observed C–Br fission from the 248 nm photodissociation of bromopropionyl chloride could result from either of these overlapping transitions. Since the addition of a single CH_2 spacer in bromopropionyl chloride vs bromoacetyl chloride should not change the general shape of the excited state potential energy surfaces in the C–Br coordinate very much, the forces along the C–Br bond fission reaction coordinate and the translational energy distributions for C–Br fission resulting from each of the two electronic transitions should be similar for the two molecules. Figure 8 shows the $P(E_T)$ characteristic of C–Br fission from excitation in the overlapping $[n_p(Br),\sigma^*(C–Br)]$ absorption, obtained in the deconvolution of the bromoacetyl chloride $P(E_T)$, superimposed on the $P(E_T)$ for C–Br bond fission in bromopropionyl chloride. The similarity between the two $P(E_T)$'s is striking, suggesting that nearly all of the observed C–Br bond fission in bromopropionyl chloride results from the $[n_p(Br),\sigma^*(C–Br)]$ transition and that none of it results from dissociation on the lowest singlet A'' surface reached with the $^1[n(O),\pi^*(C{=}O)]$ transition. The lack of C–Br bond fission upon excitation to the $^1A''$ surface is even more striking than in bromoacetyl chloride; the reason for this is developed in Sec. IV C below and in Sec. V.

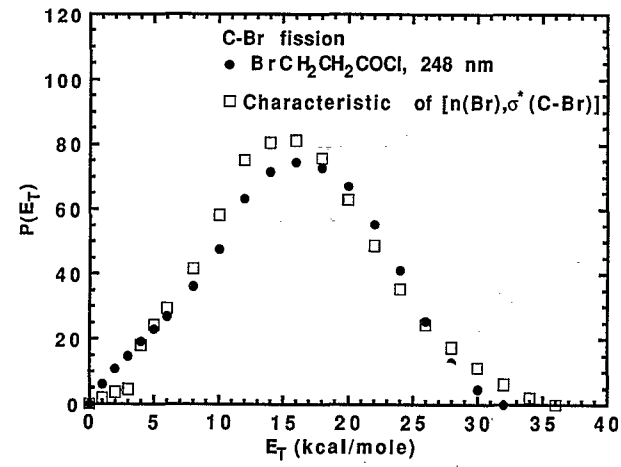

FIG. 8. A comparison between the $P(E_T)$ for the C–Br fission channel in bromopropionyl chloride at 248 nm (closed circles) with a $P(E_T)$ characteristic of C–Br fission resulting from only the overlapping $n_p(Br)\rightarrow\sigma^*(C–Br)$ transition (squares). The $P(E_T)$ shown in squares was arrived at in Fig. 7 by subtracting the $P(E_T)$ for C–Br fission in bromoacetone (Fig. 7), which results only from an $n(O)\rightarrow\pi^*(C{=}O)$ transition, from the $P(E_T)$ for C–Br fission in bromoacetyl chloride (Fig. 7) which results from overlapping $n_p(Br)\rightarrow\sigma^*(C–Br)$ and $n(O)\rightarrow\pi^*(C{=}O)$ transitions. The close match between the $P(E_T)$ for C–Br fission in bromopropionyl chloride and the one characteristic of the overlapping $n_p(Br)\rightarrow\sigma^*(C–Br)$ transition suggests that almost all of the C–Br fission in bromopropionyl chloride at 248 nm results from this $n_p(Br)\rightarrow\sigma^*(C–Br)$ transition and that little or none results from the $n(O)\rightarrow\pi^*(C{=}O)$ transition.

We measure the angular distribution of the Br and Cl fragments from bromopropionyl chloride to determine the

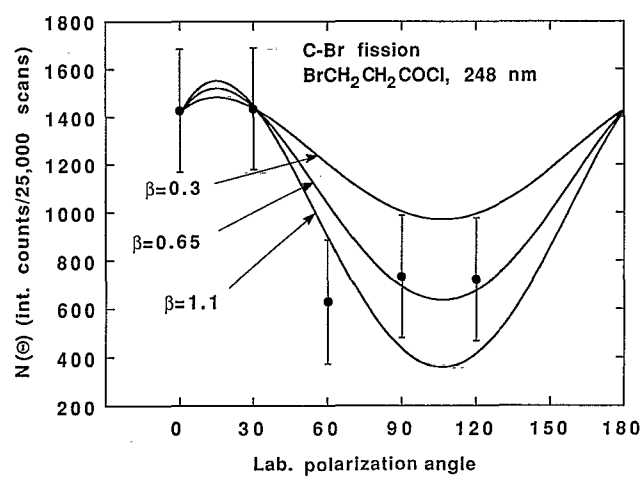

FIG. 9. Laboratory angular distribution of the Br atom product from bromopropionyl chloride photodissociated at 248 nm with linearly polarized light. Θ is the angle of the laser electric vector with respect to the detector axis (measured in the opposite sense of rotation as the source angle). The data points represent the integrated experimental TOF signal measured at five different laser polarization angles. The data points represent signal integrated between 166 and 288 μs, corresponding to laboratory velocities of 18.0 to 29.0×10^4 cm/s. Line fits show the predicted change in detected scattered signal intensity with laser polarization angle obtained, after transformation from the center of mass to the lab frame, with three trial anisotropy parameters of $\beta=1.1$, $\beta=0.65$, and $\beta=0.3$.

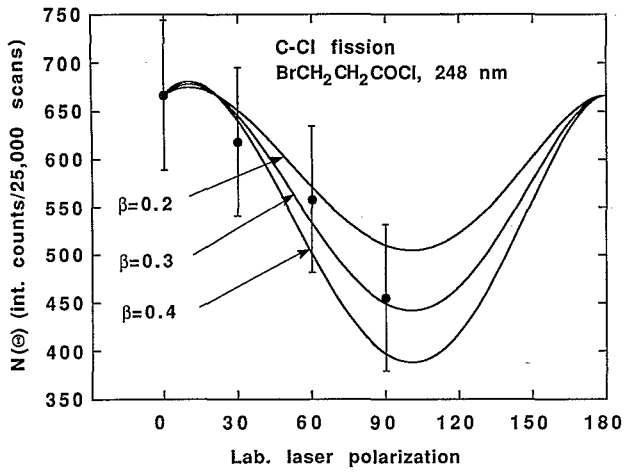

FIG. 10. Laboratory angular distribution of the Cl atom product from bromopropionyl chloride photodissociated at 248 nm with linearly polarized light. Θ is the angle of the laser electric vector with respect to the detector axis (measured in the opposite sense of rotation as the source angle). The data points represent the integrated experimental TOF signal measured at four different laser polarization angles. The data points represent signal integrated between 152 and 224 μs, corresponding to laboratory velocities of 22.7 to 36.2×10^4 cm/s. Line fits show the predicted change in detected scattered signal intensity with laser polarization angle obtained, after transformation from the center of mass to the lab frame, with three trial anisotropy parameters of $\beta=0.2$, $\beta=0.3$, and $\beta=0.4$.

time scale of C–Br and C–Cl bond fission with respect to molecular rotation and the orientation of the electronic transition dipole moment. Figure 9 shows the integrated Br fragment signal vs θ_{LAB}, the angle between the laser electric vector and the detector axis from bromopropionyl chloride photodissociation at 248.5 nm. The best fit to the photofragment angular distribution is obtained by varying the anisotropy parameter, β, in the classical electric dipole expression[13]

$$\omega(\theta_{\mathrm{C.M.}})=(1/4\pi)[1+\beta P_2(\cos\theta_{\mathrm{C.M.}})]$$

Because $\theta_{\mathrm{C.M.}}$ is the angle between the recoil direction of the detected fragment in the center-of-mass reference frame and the electric vector of the light, fitting the data involves converting between the center-of-mass and lab frames using the measured molecular beam velocity and the $P(E_T)$ derived from the unpolarized data. Measurement of the angular distribution of the Br^+ signal is consistent with the assignment of the C–Br $P(E_T)$ for bromopropionyl chloride (Figs. 4 and 8) to the $[n_p(\mathrm{Br}),\sigma^*(\mathrm{C\text{–}Br})]$ transition. Although the signal to noise is poor in our Br^+ spectra obtained with polarized light, the forward convolution fit of the fast portion of the Br^+ signal gives an anisotropy parameter, β, between 0.3 and 1.1, showing the angular distribution is roughly parallel. This roughly parallel angular distribution is similar to that of CH_2BrI excited at 248 nm for C–Br fission following $[n_p(\mathrm{Br}),\sigma^*(\mathrm{C\text{–}Br})]$ excitation.[14]

Figure 10 shows the integrated Cl atom signal vs θ_{LAB} for bromopropionyl chloride excited at 248 nm. The best fit to the Cl atom angular distribution gave a nearly isotropic $\beta=0.3\pm0.2$. One can predict what the anisotropy parameter would be if the transition dipole moment were the same as that for the $^1n(\mathrm{O})\pi^*(\mathrm{C{=}O})$ transition in acetyl and bromoacetyl chloride in the limit that photofragment recoil is axial (along the C–Cl bond direction) and prompt with respect to molecular rotation. The orientation of the $^1[n(\mathrm{O}),\pi^*(\mathrm{C{=}O})]$ transition moment in bromoacetyl chloride,[7] a transition vibronically allowed by the out of plane bend, is in the O=C–Cl plane and perpendicular to the C=O group. The angle between this transition moment and the direction of photofragment recoil along the C–Cl bond, using the ground state equilibrium geometry of bromopropionyl chloride[15] ($\angle$O=C–Cl=121.5), is $\alpha=31.5°$, resulting in a predicted anisotropy parameter[16] of $\beta=2P_2(\cos\alpha)=1.2$. Given the similarities in the $P(E_T)$'s for C–Cl bond fission in acetyl, bromoacetyl, and bromopropionyl chloride excited at 248 nm, the dynamics leading to C–Cl fission should be similar for the three molecules. Thus the marked deviation of the predicted $\beta=1.2$ for C–Cl fission in bromopropionyl chloride from the experimental value of $\beta=0.3$ is at first quite surprising. Yet, the predicted value of $\beta=1.2$ results from assuming the electronic transition is governed by the local C_{2v} symmetry of the carbonyl group, since in C_{2v} symmetry the vibronically allowed transition dipole moment is in the molecular plane and perpendicular to the C=O axis. While the local C_{2v} symmetry alone governs the electronic transition in acetyl and bromoacetyl chloride, it apparently does not govern the same $^1[n(\mathrm{O}),\pi^*(\mathrm{C{=}O})]$ transition in bromopropionyl chloride. If one considers the reduction in the symmetry from C_{2v} to C_S, the $^1[n(\mathrm{O}),\pi^*(\mathrm{C{=}O})]$ electronic transition becomes dipole allowed with a transition dipole moment perpendicular to the O=C–Cl plane. Consequently, if the electronic transition is governed by C_S symmetry, the orientation of the transition dipole moment now lies 90° from the C–Cl axis resulting in a predicted $\beta=2P_2(\cos 90°)=-1.0$. The experimentally observed $\beta=0.3$, then, likely results from a mixture of the C_{2v} vibronically allowed and the C_S dipole allowed $^1[n(\mathrm{O}),\pi^*(\mathrm{C{=}O})]$ transition. Thus, while the local C_{2v} symmetry alone adequately describes the electronic transition in acetyl and bromoacetyl chloride, the additional CH_2 spacer in bromopropionyl chloride may begin to reduce symmetry to C_S, resulting in a $^1[n(\mathrm{O}),\pi^*(\mathrm{C{=}O})]$ electronic transition governed by contributions from both the C_{2v} and C_S allowed transitions.

3. Determination of the branching ratio between C–Cl and C–Br fission

To determine the branching ratio between C–Cl and C–Br fission upon excitation of bromopropionyl chloride at 248 nm, we measured the integrated signal intensity at $^{79}Br^+$ and $^{35}Cl^+$ and accounted for all kinematic, ionization cross section, and isotope abundancy factors. To average out systematic errors, the TOF spectra at Br^+ and Cl^+ were integrated for an equal number of laser shots, changing the mass every 25 000 shots for a total of 975 000 laser shots each. The TOF signal in the raw data was integrated from 160 to 224 μs for Cl^+ and 202 to 274 μs for Br^+. This gave 0.1379 counts/shot at Br^+ and 0.0397

counts/shot at Cl^+. To calculate the absolute branching ratio between primary C–Cl and C–Br fission from the integrated signal intensities at the two ions, we begin by correcting these integrated signals, $N^{X^+}(10°)$ for ion X^+ (X=Cl,Br) measured at the source angle of 10°, for ionization cross section and isotopic abundances[17]

$$\frac{N_{\text{lab}}^{\text{Cl atoms}}(10°)}{N_{\text{lab}}^{\text{Br atoms}}(10°)}=\frac{N_{\text{lab}}^{\text{Cl}^+}(10°)\sigma_{\text{ion}}^{\text{Br}}f(^{79}\text{Br/Br})}{N_{\text{lab}}^{\text{Br}^+}(10°)\sigma_{\text{ion}}^{\text{Cl}}f(^{35}\text{Cl/Cl})}. \quad (4)$$

The relative abundances of the ^{35}Cl and ^{79}Br isotopes, $f(^{35}Cl/Cl)$ and $f(^{79}Br/Br)$, used were 0.7577 and 0.5069, respectively, and the relative ionization efficiencies, σ_{ion}, of the atoms were estimated from the atomic polarizabilities.[18] Then, to correct the flux of neutral product atoms detected in the TOF spectra for the angular and velocity distribution of the scattered products, the Jacobean factors in the conversion from center-of-mass to laboratory scattering frame, and flux measured in time versus kinetic energy space, we used a standard program, RPCMLAB3,[19] to calculate f_{diff}^{X}, the expected signal at each mass given a 1:1 branching ratio. Correcting for this relative differential scattering efficiency gives the final product branching ratio as

$$\text{Primary product branching ratio}\frac{\text{C–Cl fission}}{\text{C–Br fission}}$$

$$=\frac{N_{\text{lab}}^{\text{Cl atoms}}(10°)f_{\text{diff}}^{\text{Br}}(10°)}{N_{\text{lab}}^{\text{Br atoms}}(10°)f_{\text{diff}}^{\text{Cl}}(10°)}. \quad (5)$$

The final result was a primary product branching ratio of C–Cl:C–Br=1.0:2.0. However, because essentially all of the C–Br fission observed is due to direct dissociation via the overlapping $n_p(\text{Br})\sigma^*(\text{C–Br})$ transition (see Sec. IV B 2), the corrected branching ratio between C–Cl and C–Br fission resulting from $^1[n(O),\pi^*(C{=}O)]$ excitation at the carbonyl group is 1.0:<0.05.

C. Theoretical results

We calculate the energies of the singlet excited electronic states of bromopropionyl and bromoacetyl chloride to determine the splittings between the two lowest $^1A''$ electronic states at the avoided crossing in both the C–Cl and C–Br bond fission channels. Using the trans conformer of each molecule to retain the plane of symmetry, the energies of the excited states are determined along the C–Br and C–Cl stretching coordinates for a variety of C=O bond distances. For bromopropionyl chloride, cuts in the excited state potential energy surfaces are determined by independently stretching either the C–Cl or C–Br bond while fixing the C=O bond length at 1.195, 1.295, 1.395, 1.495, and 1.595 Å. Similarly for bromoacetyl chloride, cuts along the C–Br and C–Cl stretching coordinates are taken with the C=O bond length at 1.188, 1.313, 1.388, and 1.588 Å. Table I summarizes the results of the calculation by showing the energy of the lowest $^1A''$ excited electronic state and the splitting between the two lowest $^1A''$ surfaces at the point of the avoided crossing in the various one-dimensional cuts which were calculated.

TABLE I. Summary of *ab initio* calculations of the barriers along the C–Cl and C–Br bond fission reaction coordinates, at a variety of C=O bond lengths, in bromoacetyl and bromopropionyl chloride. The first three columns give the C=O, C–Br, and C–Cl bond lengths, in Å, at the barrier. The fourth column shows the calculated energy of the lowest $^1A''$ adiabatic electronic surface at the barrier, while the fifth column, labeled $2V_{12}$, shows the splitting between the two lowest $^1A''$ states at the barrier.

Bromoacetyl chloride

Barrier to C-Cl bond fission

$R_{(C=O)}$	$R_{(C-Br)}$	$R_{(C-Cl)}$ at barrier	Energy (cm^{-1}) at barrier on $^1A''$, referenced to minimum in the ground state	$2V_{12}$ (cm^{-1})
1.188	1.935	2.232	50548	401.7
1.313	1.935	2.382	44192	88.7
1.388	1.935	2.464	44763	57.3
1.588	1.935	2.553	53264	1160.0

Barrier to C-Br bond fission

$R_{(C=O)}$	$R_{(C-Br)}$ at barrier	$R_{(C-Cl)}$	Energy (cm^{-1}) at barrier on $^1A''$, referenced to minimum in the ground state	$2V_{12}$ (cm^{-1})
1.188	2.3205	1.789	46136	225.0
1.313	2.522	1.789	40051	137.9
1.388	2.627	1.789	40821	121.0
1.588	2.777	1.789	50513	67.8

Bromopropionyl chloride

Barrier to C-Cl bond fission

$R_{(C=O)}$	$R_{(C-Br)}$	$R_{(C-Cl)}$ at barrier	Energy (cm^{-1}) at barrier on $^1A''$, referenced to minimum in the ground state	$2V_{12}$ (cm^{-1})
1.195	1.935	2.239	50897	404.1
1.295	1.935	2.351	45335	130.6
1.395	1.935	2.453	45296	106.5
1.495	1.935	2.523	48279	494.4

Barrier to C-Br bond fission

$R_{(C=O)}$	$R_{(C-Br)}$ at barrier	$R_{(C-Cl)}$	Energy (cm^{-1}) at barrier on $^1A''$, referenced to minimum in the ground state	$2V_{12}$ (cm^{-1})
1.195	2.3439	1.797	47536	22.6
1.295	2.503	1.797	41698	20.2
1.395	2.626	1.797	41324	12.1
1.495	2.7247	1.797	44550	9.7

In general, the calculated energy of the lowest $^1A''$ surface at the barrier to either C–Cl or C–Br bond fission is higher than the 248.5 nm or 40241.4 cm^{-1} experimental photon energy, although the barrier to C–Br fission in bromoacetyl chloride with a 1.313 Å C=O bond length is slightly below the photon energy. The *ab initio* CIS and CISD calculations with the relatively small STO-3G* basis set obviously give excited state energies which are too high. (More accurate energy surfaces could be produced if substantially larger basis sets were to be used and if the number of configurations included in the CI were increased.) Subtracting a constant amount from the excited electronic states at all geometries so that the calculated energy of the $^1[n(O),\pi^*(C{=}O)]$ electronic transition from the equilibrium ground state geometry matches the center of the experimental absorption spectrum still does not lower the barriers to C–Cl and C–Br bond fission below the experimental photon energy. For instance, the peak of the $^1[n(O),\pi^*(C{=}O)]$ transition in bromopropionyl chloride experimental absorption spectra occurs at 260 nm or 38 462 cm^{-1}. The calculated $^1[n(O),\pi^*(C{=}O)]$ excitation energy from the equilibrium ground state geometry is 40 468.6 cm^{-1}. Even lowering the excited electronic states by this 2000 cm^{-1} difference will not lower the barrier to

C–Cl fission below the photon energy, although it will lower that to C–Br fission for selected C=O bond distances.

Although the calculated barriers are too high in absolute energy, the *ab initio* calculations still provide valuable insight into the photodissociation of bromopropionyl and bromoacetyl chloride. For both bromopropionyl and bromoacetyl chloride the calculations clearly show that the barrier to C–Cl fission results from an avoided crossing between an electronic state with predominant $^1n(O)\pi^*(C{=}O)$ electronic configuration and one with mainly $n_p(Cl)\sigma^*(C–Cl)$ electronic configuration. Similarly, the calculations show that the barrier to C–Br fission results from an avoided crossing of states with mainly $^1n(O)\pi^*(C{=}O)$ and $n_p(Br)\sigma^*(C–Br)$ electronic character. In addition, as Table I shows, for both bromopropionyl and bromoacetyl chloride, at all C=O bond distances examined, the adiabatic barrier to C–Cl bond fission is consistently higher than the one to C–Br bond fission, on average by greater than 10 kcal/mol. This confirms the intuitive aspects of our previous model for bromoacetyl and bromopropionyl chloride photodissociation which suggested that the barrier to C–Cl fission was higher, on the lowest $^1A''$ adiabatic electronic surface, than the barrier to C–Br fission. The theoretical potential energy surface also shows that the difference in the heights of the barrier to C–Cl and C–Br bond fission changes as a function of the C=O bond length, being larger at contracted C=O bond distances and smaller at extended C=O bond distances.

Thus, given that the barrier to C–Cl fission is higher than the barrier to C–Br bond fission at all geometries sampled on the lowest $^1A''$ adiabat, we can qualitatively address the predictions of statistical theories using only the single adiabatic electronic surface. Statistical theories assume that the rate, k, of adiabatic passage across an energetic barrier is $k=A\exp(-E_a/k_bT)$,[20] where A is the Arrhenius pre-exponential entropic factor, E_a is close to the barrier height relative to the well in the adiabatic surface, k_b is Boltzman's constant, and T is the temperature. Although the absolute barrier heights from our *ab initio* calculations were too crude to allow us to predict a C–Cl:C–Br branching ratio or equivalently the ratio of k(C–Cl):k(C–Br), the barrier to C–Cl fission is about 10 kcal/mol higher than the barrier to C–Br fission. Consequently, predictions based only on a single adiabatic potential energy surface will always predict more C–Br fission than C–Cl fission. The experimentally observed C–Cl:C–Br branching ratio of 1.0:0.4 in bromoacetyl chloride and 1.0:$<$0.05 in bromopropionyl chloride clearly indicates that we must go beyond considering only the lowest adiabatic potential energy surface and also consider the important nonadiabatic couplings at the avoided crossings which form the barriers to C–Cl and C–Br bond fission.

While the experimentally observed C–Cl:C–Br branching ratios cannot be understood on the basis of the relative barrier heights on the lowest $^1A''$ adiabatic potential energy surface, they can be understood by examining the relative *magnitude* of the nonadiabatic coupling at the barriers formed from avoided crossings. When the splitting between adiabats at the avoided crossing is small, there is a high probability that the molecules will retain their original electronic configuration, "hop" to the upper adiabat, and then possibly return into the Franck–Condon region. For bromopropionyl chloride, the calculations show that the splitting between adiabats at the avoided crossing which forms the barrier to C–Cl fission is consistently larger than the splitting at the barrier to C–Br fission. Consequently, the dynamics leading to C–Cl bond fission are more likely to adiabatically pass over the barrier to C–Cl fission. The much smaller splitting at the avoided crossing forming the barrier to C–Br fission implies that the nuclear dynamics which sample the barrier to C–Br fission are more likely to nonadiabatically hop to the upper adiabat at the avoided crossing. This nonadiabatic transition results in a decreased probability of adiabatic passage through the barrier to C–Br bond fission and, consequently, a decreased probability of C–Br fission.

For bromoacetyl chloride, the situation is less clear cut, but the relative energetic splittings between adiabats at the two avoided crossings can still explain the experimentally observed preferential C–Cl fission. At short and long C=O bond distances, $R_{C=O}=1.188$ and 1.588 Å, respectively, Table I shows that the calculated splitting between the adiabats at the barrier to C–Cl bond fission is significantly larger than the splitting between the adiabats at the barrier to C–Br bond fission. Thus at relatively long and short C=O bond distances, the larger splitting between adiabats at the barrier to C–Cl fission results in a higher probability of adiabatic passage through the barrier to C–Cl fission and increased C–Cl bond fission relative to C–Br bond fission. On the other hand, at intermediate C=O bond distances, $R_{C=O}=1.313$ and 1.388 Å, the calculated splitting between the adiabats at the barrier to C–Cl fission is actually smaller than the splitting between adiabats at the barrier to C–Br fission. The equilibrium C=O bond distance in the ground electronic state is near 1.188 Å while the equilibrium C=O bond length in the lowest $^1A''$ excited electronic state, reached upon the $^1n(O)\pi^*(C{=}O)$ electronic transition, is near 1.313 Å. Thus the initial Franck–Condon transition results in a C=O bond which is displaced from its equilibrium position on the electronically excited $^1A''$ surface. As a result, the molecule experiences significant stretching force in the $R_{C=O}$ coordinate. Because of this excitation of the C=O stretching vibration, the nuclear dynamics is likely to sample the barriers to both C–Cl and C–Br bond fission with significant C=O vibrational excitation. This implies that the nuclear dynamics preferentially samples the avoided crossings at short, $R_{C=O}=1.188$ Å, and long, $R_{C=O}=1.588$ Å, C=O bond lengths, where the splitting between adiabats at the C–Cl barrier is larger than at the barrier to C–Br fission. Thus, because the nuclear dynamics preferentially samples the avoided crossing where the splitting between adiabats at the barrier to C–Cl bond fission is relatively large, there is a higher probability of passing through the barrier to C–Cl fission adiabatically and consequently a higher probability of C–Cl bond fission. In addition, even the nuclear dynamics which sample the

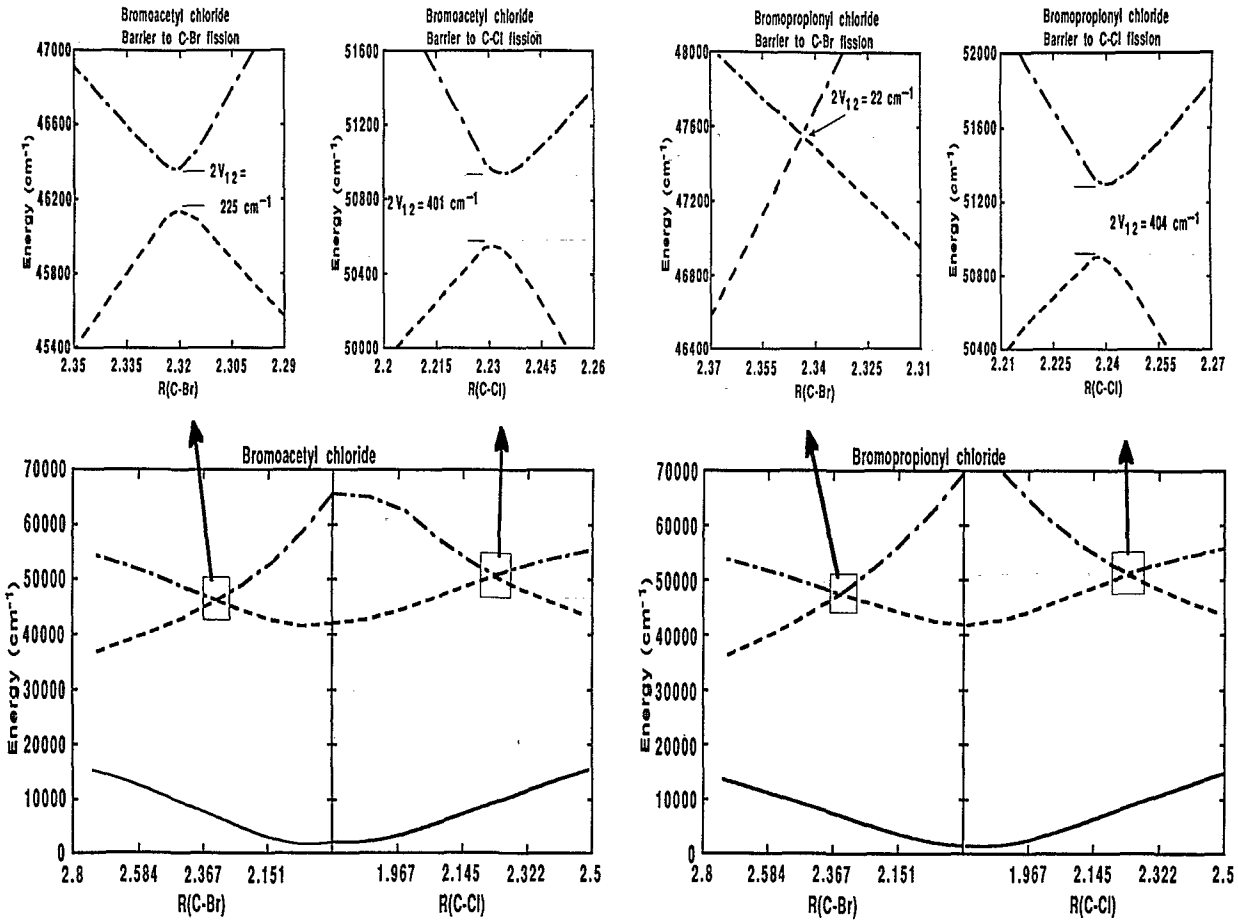

FIG. 11. Cuts through the calculated *ab initio* electronic surfaces for bromoacetyl chloride (left) with $R(C{=}O) = 1.188$ and bromopropionyl chloride (right) with $R(C{=}O) = 1.195$. The boxed-in portions at the barrier to each bond fission pathway, which are enlarged in the insets above each, show that the probability of C–Br bond fission decreases in bromopropionyl chloride because the splitting between adiabats at the barrier to C–Br bond fission decreases by a factor of ten from that in bromoacetyl chloride. The smaller adiabatic splitting at the barrier to C–Br bond fission in bromopropionyl chloride results in a higher probability of nonadiabatic recrossing of the barrier and suppression of C–Br bond fission. For the particular cut along the avoided crossing seam shown here, the splitting at the avoided crossing to C–Br fission reduces from 225 cm^{-1} in bromoacetyl chloride to 22 cm^{-1} in bromopropionyl chloride. Other cuts are given in Table I.

avoided crossings at the excited state equilibrium C=O bond distance, $R_{C=O} = 1.313$ Å, where the splitting between adiabats at the barrier to C–Cl fission is smaller, may still lead to preferential C–Cl bond fission because of the relatively small velocity through the crossing at the high energy barrier to C–Cl fission.

Of more central concern to this paper, the calculated splittings between the adiabats at the barrier to C–Br fission also qualitatively explain the dramatically decreased probability of C–Br bond fission in bromopropionyl chloride versus bromoacetyl chloride. For all C=O bond distances at the barrier to C–Br bond fission, the splitting between the adiabats shown in Table I and Fig. 11 is nearly ten times larger in bromoacetyl chloride than in bromopropionyl chloride. The larger splitting in bromoacetyl chloride implies that the nuclear dynamics have a higher probability of adiabatically passing through the barrier to C–Br fission in bromoacetyl chloride than in bromopropionyl chloride. In bromopropionyl chloride, the smaller splitting of only 10 to 20 cm^{-1} at the avoided crossing leading to C–Br fission results in a larger probability of retaining the initial $^1n(O)\pi^*(C{=}O)$ electronic configuration by making a nonadiabatic transition to the upper adiabat, and thereby suppressing the probability of C–Br bond fission. Thus, the smaller splitting between adiabats at the barrier to C–Br bond fission in bromopropionyl chloride predicts a decreased probability of branching to the C–Br bond fission channel in bromopropionyl chloride vs bromoacetyl chloride. This is just the change observed experimentally where the C–Br:C–Cl bond fission ratio decreases from 0.4:1.0 for bromoacetyl chloride to <0.05:1.0 in bromopropionyl chloride.

V. DISCUSSION

A. Overview

The experimental results presented above clearly show that increasing the distance between the C=O and C–Br chromophores, by inserting an additional CH_2 spacer on going from bromoacetyl to bromopropionyl chloride, results in essentially complete suppression of C–Br bond fission following an initial $^1[n(O),\pi^*(C{=}O)]$ electronic

transition. In addition, the calculations also show that this suppression of C–Br bond fission in bromopropionyl chloride results because of the very small 10 to 20 cm^{-1} splitting between adiabats at the barrier to C–Br bond fission. In the discussion below we first show how this suppression of C–Br bond fission in bromopropionyl chloride reemphasizes the lack of predictive ability for the branching between C–Cl and C–Br bond fission when considering only the lowest adiabatic excited electronic surface. Then we show how incorporating nonadiabatic effects explains the suppression of C–Br bond fission in bromopropionyl chloride, where the effect is pronounced because the matrix elements responsible for the off-diagonal potential coupling at the barrier to C–Br bond fission depend strongly on the distance between the two chromophores. Then, in Sec. V D, we show that nonadiabatic effects can be important for a wide class of Woodward–Hoffmann forbidden reactions, a class to which carbon–halogen bond fission in bromoacetyl and bromopropionyl chloride belong, where individual orbital symmetry is not conserved along the reaction coordinate. Finally, in Sec. V E, we compare our present results with previous studies of electron transfer and triplet–triplet excitation transfer where the reaction rates are also controlled by nonadiabaticity at the reaction barrier.

B. Examining whether adiabatic dissociation along the $^1A''$ potential energy surface gives predictive ability

Our previous model for bromoacetyl chloride proposes that the C–Cl:C–Br branching ratio of 1.0:0.4 following $^1[n(O),\pi^*(C{=}O)]$ excitation cannot be explained on the basis of a single Born–Oppenheimer adiabatic potential energy surface. The experimental C–Cl:C–Br branching ratio of 1.0: <0.05 following the same $^1[n(O),\pi^*(C{=}O)]$ excitation in bromopropionyl chloride further emphasizes the lack of predictive ability when considering only the lowest $^1A''$ adiabatic surface. Figure 1 shows the schematic adiabatic reaction coordinates for bromoacetyl and bromopropionyl chloride photodissociation while Fig. 11 shows cross sections through our calculated potential energy surfaces. Since the barrier to C–Cl bond fission is higher than the barrier to C–Br bond fission on the lowest $^1A''$ adiabat, statistical theories considering only this adiabat wrongly predict preferential C–Br bond fission for both of these systems. This alone suggests that considering solely the single lowest $^1A''$ adiabatic surface can not explain the observed preferential C–Cl bond fission. However, the preferential C–Cl fission might conceivably result on the single adiabat if the zeroth order vibrational states initially excited were coupled more strongly through intramolecular vibrational energy redistribution (IVR) to the C–Cl stretching coordinate than to the C–Br stretching coordinate. If this were the case the dynamics would sample the barrier to C–Cl fission more often than the barrier to C–Br bond fission, possibly resulting in preferential C–Cl bond fission even though the barrier to C–Cl bond fission is approximately 10 kcal/mol higher than the barrier to C–Br bond fission. But, since the only difference between bromoacetyl and bromopropionyl chloride is one CH_2 spacer, the forces along the lowest $^1A''$ excited electronic state and the coupling of the initially excited vibrational states to the C–Br stretching coordinate should be similar for the two molecules, so both reaction barriers should be accessed statistically. Although the additional CH_2 spacer in bromopropionyl chloride might decrease coupling to the C–Br stretching coordinate by a small amount, it is not reasonable to assume that C–Br bond fission would decrease by a factor of 10 or more in bromopropionyl chloride if IVR alone were responsible for the dynamics. To isolate the C–Br vibrational mode this effectively, one would need to repace the C–C spacer with a very high frequency oscillator such as an acetylenic C≡C bond.[21] Consequently, the results on bromopropionyl chloride confirm our earlier conclusions for bromoacetyl chloride: we must consider nonadiabatic effects near the barrier to each bond fission channel in order to understand the observed C–Cl:C–Br branching ratios in bromoacetyl and bromopropionyl chloride. In the next section we show how the rate constant for crossing the adiabatic barrier to C–Br fission is reduced in bromopropionyl chloride vs bromoacetyl chloride due to decreased electron correlation between the $^1n(O)\pi^*(C{=}O)$ and $n_p(Br)\sigma^*(C\text{–}Br)$ configurations.

C. The influence of nonadiabaticity on the C–Cl:C–Br branching ratio in bromopropionyl vs bromoacetyl chloride

The barriers along the $^1A''$ adiabat in Figs. 1 and 11 implicitly result from the avoided crossing of the $^1n(O)\pi^*(C{=}O)$ and $n_p(X)\sigma^*(C\text{–}X)$ electronic configurations, where X=Cl or Br. Consequently, transitions to higher adiabatic potential energy surfaces, shown schematically in Fig. 1 and in cross sections of our *ab initio* calculations in Fig. 11, are possible at each avoided crossing. If one retains the internal nuclear coordinate derivative coupling in the full Schrödinger equation, then the smaller the energy splitting between the higher and lower adiabats at the barrier, the larger the probability that the molecule will hop to the upper adiabat as it attempts to cross the barrier to C–Cl or C–Br fission. We explain below why we expect the splitting between the adiabats at the barrier to C–Br fission to be smaller in bromopropionyl chloride than in bromoacetyl chloride, providing the reason for the marked decrease in C–Br bond fission in bromopropionyl chloride.

In the simplified approximately diabatic representation shown in the lower frame in Fig. 1, the nonadiabatic hop is represented by the molecule retaining the $^1n(O)\pi^*(C{=}O)$ electronic configuration at the curve crossing and climbing the C–Br attractive wall until it turns back toward the Franck–Condon region. In this simple diabatic picture where each diabatic state is represented by a single molecular electronic configuration, the off-diagonal potential coupling between the two electronic states can come from two kinds of matrix elements, both corresponding to electron correlation between the pairs of orbitals involved. The matrix elements responsible for the off-diagonal potential coupling are of the form[22]

$$2\left\langle n_O(1)n_{Br}(2)\left|\frac{e^2}{r_{12}}\right|\pi^*_{C=O}(1)\sigma^*_{C-Br}(2)\right\rangle \quad (6)$$

and

$$\left\langle n_O(1)\pi^*_{C=O}(2)\left|\frac{e^2}{r_{12}}\right|n_{Br}(1)\sigma^*_{C-Br}(2)\right\rangle. \quad (7)$$

The first term, the dipole–dipole coupling term, is proportional to $1/R^3$ at long distances, where R is the separation between the two transition dipole moments. Both matrix elements become smaller as the distance between the C=O chromophore and the C–Br bond increases. The first term obviously becomes smaller with increasing separation, r, and the second term becomes smaller because the overlap densities $n_O(1)n_{Br}(1)$ and $\pi^*_{C=O}(2)\sigma^*_{C-Br}(2)$ decrease. Consequently, this simple approximation to the coupling matrix elements provides qualitative understanding of the changes in branching to the C–Br bond fission channel in bromopropionyl chloride. Increasing the distance between the C=O chromophore and the C–Br bond, by inserting a CH_2 spacer, results in decreased electron correlation between the two electronic configurations. Due to the decreased electron correlation between the $^1n(O)\pi^*(C{=}O)$ and $n_p(Br)\sigma^*(C–Br)$ configurations, when bromopropionyl chloride samples the barrier to C–Br bond fission, it has a much higher probability of retaining the initial $^1n(O)\pi^*(C{=}O)$ electronic configuration (Fig. 1) and then returning toward the Franck–Condon region. Consequently, we see a marked decrease in C–Br bond fission in bromopropionyl chloride in comparison with bromoacetyl chloride. Similarly, in the adiabatic picture the decreased electron correlation in bromopropionyl chloride results in a much smaller energetic splitting between the adiabats at the barrier to C–Br bond fission, as shown in our *ab initio* calculations in Fig. 11. The smaller splitting between the adiabats increases the probability of a nonadiabatic hop to the upper surface, thereby decreasing the probability of C–Br bond fission.

D. Factors determining the importance of nonadiabaticity in chemical reactions

At first glance it might be quite surprising that nonadiabatic effects would so heavily favor C–Cl bond fission in both bromopropionyl and bromoacetyl chloride even though the barrier to C–Cl bond fission is approximately 10 kcal/mol higher than the barrier to C–Br bond fission. A closer examination of the electronic crossings which form the barriers to C–Cl and C–Br fission, however, reveals why these and other systems should evidence such a dramatic failure of the Born–Oppenheimer approximation. Woodward and Hoffmann's[23] work outlined a class of chemical reactions, those for which overall symmetry is conserved along the reaction coordinate but individual orbital symmetry is not, that typically have large barriers along the reaction coordinate. The simple model below shows that in Woodward–Hoffmann forbidden reactions, not only is there a barrier along the reaction coordinate, but also the probability of adiabatically crossing this barrier for trajectories with sufficient energy to do so is dramatically reduced by nonadiabatic effects.

As in the previous section, consider the dominant electronic configuration contributing to the electronic wave function, Ψ_R, on the reactant side of the barrier, represented by one electron in an n_O orbital and another in a $\pi^*_{C=O}$ orbital, and the dominant configuration contributing to the electronic wave function, Ψ_P, on the product side of the barrier, represented by one electron in a n_X orbital and one in a σ^*_{C-X} orbital (where X=Cl or Br). Thus the electronic configuration on the reactant side of the barrier $\{\cdots(n_X)^2(n_O)^1(\pi^*_{C=O})^1(\sigma^*_{C-X})^0\}$, differs from that on the product side of the barrier $\{\cdots(n_X)^1(n_O)^2(\pi^*_{C=O})^0(\sigma^*_{C-X})^1\}$, by two electrons. Configuration interaction matrix elements mix and split these two electronic configurations at the avoided crossing which forms the barrier to C–X bond fission. In this two state model, the general expression (if no orthogonality is assumed between reactant and product molecular orbitals or between Ψ_R and Ψ_P) for the splitting between the adiabatic Born–Oppenheimer potential energy surfaces is[24]

$$\text{Splitting}=2V_{12}=2(\beta-\alpha S)(1-S^2)^{-1}, \quad (8)$$

where α is the energy at which the diabats cross, S is the overlap integral $\langle\Psi_R|\Psi_P\rangle/C$, β is the interaction, resonance, or exchange energy $\langle\Psi_R|\mathscr{H}|\Psi_P\rangle/C$, and C corrects for unnormalized wavefunctions. However, for Woodward–Hoffmann forbidden reactions, like C–Cl and C–Br bond fission on the lowest $^1A''$ electronic state of bromoacetyl and bromopropionyl chloride, the overlap integral, S, is zero because individual orbital symmetry is not conserved. In planar C_S bromoacetyl and bromopropionyl chloride, the $\pi^*_{C=O}$ orbital has a'' symmetry while the σ^*_{C-X} orbital has a' symmetry so the overlap integral $\langle\pi^*_{C=O}|\sigma^*_{C-X}\rangle = \langle a''|a'\rangle = 0$. Similarly, the n_X orbital has a'' symmetry while the n_O orbital has a' symmetry so the overlap integral $\langle n_X|n_O\rangle=\langle a''|a'\rangle=0$. Because individual orbital symmetry is not conserved for Woodward–Hoffmann forbidden reactions, all one electron integrals that contribute to the resonance and exchange energy represented by β above are also zero, leaving only two electron integrals to mix and split the electronic states at the avoided crossing.[24] The splitting between the adiabats at the barrier (equal to twice the off-diagonal potential coupling between two diabatic electronic configurations in the diabatic representation) is, for singlets[22]

$$2V_{12}=2[\underbrace{2\langle n_O(1)n_X(2)|e^2/r_{12}|\pi^*_{C=O}(1)\sigma^*_{C-X}(2)\rangle}_{\text{Förster}} - \underbrace{\langle n_O(1)\pi^*_{C=O}(2)|e^2/r_{12}|n_x(1)\sigma^*_{C-X}(2)\rangle}_{\text{Dexter}}. \quad (9)$$

To summarize, because all overlap integrals and one electron integrals are zero in these Woodward–Hoffmann forbidden reactions, bromoacetyl and bromopropionyl chloride have anomolously small splittings between the adiabats at the barrier to carbon–halogen bond fission. As a result of these small splittings at the barriers to C–Cl and C–Br bond fission, nonadiabatic recrossing of the barrier

plays a dominant role in controlling the relative probability of C–Cl and C–Br bond fission. In the case of bromopropionyl and bromoacetyl chloride presented here, the smaller splitting at the barrier to C–Br bond fission leads to a higher probability of nonadiabatic recrossing of the barrier to C–Br bond fission, suppression of C–Br bond fission, and consequently a preferential fission of the C–Cl bond.

Silver[24] recognized, nearly two decades ago, that Woodward–Hoffmann forbidden reactions, like carbon–halogen bond fission on the lowest $^1A''$ electronic state in bromopropionyl and bromoacetyl chloride, should evidence anomalously small splittings between adiabats at the reaction barrier. Yet Silver interpreted these results merely in terms of their effect on the energetic height of the barrier on the lowest adiabatic electronic surface. Silver explained the low reaction rates in Woodward–Hoffmann forbidden reactions, for example, as resulting from the increased energetic barrier on the lowest adiabatic surface. While the smaller than expected splitting between adiabats at a barrier in a Woodward–Hoffmann forbidden reaction does result in slightly increased barrier heights, the present results on bromoacetyl and bromopropionyl chloride dramatically illustrate that the increased nonadiabaticity which results from the small splittings, and not simply the increased barrier heights, accounts for the decreased reaction rates in Woodward–Hoffmann forbidden reactions. In bromopropionyl and bromoacetyl chloride, the small splittings between the adiabats at the barriers to carbon–halogen bond fission probably do raise the energetic barriers above what might be expected if individual orbital symmetry were conserved and the reaction was Woodward–Hoffman allowed. Yet in this case, even with the raising of the adiabatic barrier heights due to the small splitting between adiabats, the adiabatic barrier to C–Cl bond fission remains approximately 10 kcal/mol higher than the barrier to C–Br fission. If the relative barrier heights determined the C–Cl:C–Br branching ratio, we would obviously expect preferential C–Br fission, in marked contrast to the experimentally observed preferential C–Cl fission. Thus, the preferential C–Cl fission in bromopropionyl and bromoacetyl chloride shows that in Woodward–Hoffmann forbidden reactions, there is not only a large barrier along the reaction coordinate, but there is also a dramatically reduced probability of adiabatically crossing this barrier due to increased nonadiabatic recrossing of the barrier.

E. Geometrical factors which control the magnitude of nonadiabaticity

Having established the importance of nonadiabaticity in Woodward–Hoffmann forbidden reactions, it is interesting to consider the geometrical factors which control the magnitude of nonadiabaticity at the barrier to a reaction. This work documents the distance dependence of nonadiabaticity by comparing the probability of C–Br bond fission in bromoacetyl and bromopropionyl chloride. Increasing the distance between the C–Br and C═O chromophores decreases the electronic configuration interaction matrix elements which mix and split the $^1n(\mathrm{O})\pi^*(\mathrm{C{=}O})$ and $n_p(\mathrm{Br})\sigma^*(\mathrm{C\text{–}Br})$ configurations at the barrier to C–Br bond fission in bromopropionyl chloride. The resulting increased probability of nonadiabatic recrossing of the barrier to C–Br bond fission results in a decreased probability of C–Br bond fission in bromopropionyl chloride. Successful adiabatic passage through the barrier to C–Br bond fission in these systems results because of an implicit intramolecular electronic excitation transfer from the initially excited $^1n(\mathrm{O})\pi^*(\mathrm{C{=}O})$ configuration to the $n_p(\mathrm{Br})\sigma^*(\mathrm{C\text{–}Br})$ configuration. As we have seen in bromoacetyl and bromopropionyl chloride, the magnitude of the splitting between adiabats at the barrier to bond fission controls the rate of the implicit intramolecular electronic excitation transfer and, hence, the probability of bond fission. When the splitting between adiabats at the barrier to C–Br bond fission is larger, as in bromoacetyl chloride, the rate of intramolecular electronic excitation transfer is faster, resulting in a higher probability of C–Br bond fission.

In related work, Closs and co-workers[25] have examined the distance dependence of intramolecular electronic excitation transfer in electron transfer and triplet excitation transfer in bound bichromophoric molecules. Just as in the above case of C–Br bond fission in bromoacetyl and bromopropionyl chloride, the rates of electron transfer and triplet excitation transfer in these systems are controlled by the magnitude of the splitting between adiabats at the barrier along the reaction coordinate. For both electron transfer and triplet excitation transfer, Closs finds that the rate of intramolecular electronic excitation transfer decreases exponentially with the number of intervening bonds between the donor and acceptor chromophores. In addition, when comparing the relative rates of electron and triplet excitation transfer in the same molecule, Closs finds that the rate of triplet excitation transfer is approximately equal to the rate of electron transfer squared. In a simple model, this results because the rate of electron transfer depends on a one electron, two orbital resonance integral, while the rate of triplet excitation transfer depends on a two electron, four orbital exchange integral equivalent to the Dexter term in Eq. (9). Since the rate of triplet excitation transfer in Closs' work is controlled by the Dexter type electronic configuration interaction matrix elements, it is interesting to compare the predictions of the empirical relationship for the rate of this triplet excitation transfer, derived in Closs' work, with the present results on bromoacetyl and bromopropionyl chloride. Closs showed that the magnitude of the off-diagonal potential coupling driving intramolecular triplet excitation transfer decreased with the number of intervening bonds, N, between donor and acceptor chromophores according to the relationship $V=V_0\exp[-\alpha(N-1)/2]$, with $\alpha=2.53$. Thus with the addition of one intervening bond in going from bromoacetyl to bromopropionyl chloride, we would expect the coupling to change by a factor of $\exp(-2.53/2)=0.28$. This decrease by a factor of 3.5 in the off-diagonal potential coupling results in a predicted rate of crossing the adiabatic barrier to C–Br bond fission in bromopropionyl chloride being reduced by a factor of 12. This is consistent with the observed C–Cl:C–Br branching ratios, following

$^1n(O)\pi^*(C{=}O)$ excitation, of 1.0:0.4 in bromoacetyl chloride and 1.0: <0.05 in bromopropionyl chloride, where the probability of C–Br bond fission is reduced by at least a factor of 10 in bromopropionyl chloride. The reported branching ratio for bromopropionyl chloride, however, is an upper limit on C–Br bond fission, reflecting our lack of sensitivity to very small amounts of C–Br bond fission products, and the actual probability of C–Br bond fission in bromopropionyl chloride may be much smaller. In fact, comparison of the calculated splittings between adiabats at the barrier to C–Br bond fission in bromoacetyl and bromopropionyl chloride suggests that Closs' empirical relationship between coupling and distance actually underestimates the decrease in coupling on going from bromoacetyl to bromopropionyl chloride. The calculated splitting between adiabats at the barrier to C–Br bond fission, and hence the off-diagonal potential coupling between the $^1n(O)\pi^*(C{=}O)$ and $n_p(Br)\sigma^*(C\text{–}Br)$ configurations, is actually ten times smaller in bromopropionyl chloride than in bromoacetyl chloride. This calculated 10-fold reduction in the off-diagonal potential coupling predicts an approximately 100-fold decrease in C–Br bond fission in bromopropionyl chloride, nearly an order of magnitude greater than the decrease predicted from Closs' empirical relationship.

The discrepancy between the predictions of Closs' empirical relationship and the calculated adiabatic splittings at the barrier to C–Br bond fission in bromoacetyl and bromopropionyl chloride is actually quite surprising. Since Closs' empirical relationship was derived from studies of triplet excitation transfer, only the Dexter exchange matrix elements contribute to the off-diagonal potential coupling. Because C–Br bond fission in bromoacetyl and bromopropionyl chloride involves singlet excitation transfer, both the Dexter and Förster dipole–dipole matrix elements contribute to the off-diagonal potential coupling. Since the Förster coupling decreases more slowly with distance than the Dexter coupling, we intuitively expect the rate of singlet excitation transfer to have a smaller distance dependence than the rate of triplet excitation transfer. It is, however, possible that orientational effects may also contribute to the decreased adiabatic splitting at the barrier to C–Br bond fission in bromopropionyl chloride. Although in Closs' studies care was taken to keep the relative orientation of the donor and acceptor molecules constant for all the molecules in the series, the relative orientation of the C–Br and C=O chromophores is different in bromopropionyl chloride than in bromoacetyl chloride. Since the magnitude of the off-diagonal potential coupling also depends on the relative orientation of electronic orbitals involved in the configuration crossing, the differing orientation of the two chromophores may also be a source of the dramatically decreased probability of C–Br bond fission in bromopropionyl chloride.

In other more recent work, Speiser[26] also examines the rate of intramolecular electronic excitation transfer in bound bichromophoric molecules. For a series of molecules with nearly identical orientations of the donor and acceptor electronic orbitals, Speiser also finds that the excitation transfer rate depends exponentially on the distance between the two chromophores. Furthermore, for this series of molecules, Speiser finds that the electronic configuration interaction matrix elements that mix and split the donor and acceptor configurations at the barrier along the reaction coordinate are also best described by the Dexter term in Eq. (9).

In addition to this distance dependence, the electronic configuration interaction matrix elements also depend on the relative orientation of the electronic orbitals involved in the configuration crossing. Forthcoming work from our laboratory, which investigates the conformational dependence of the branching between C–Br and C–C bond fission in bromoacetone excited at 308 nm,[12] examines how the relative orientation of the orbitals involved influences the nonadiabaticity along the C–Br and C–C bond fission reaction coordinates. The results provide a vivid example of the effect of sampling different portions of nuclear phase space in the region of a conical intersection in the C–C bond fission coordinate. Although the *gauche* conformer of bromoacetone is nearly four times more populated than the anticonformer, we observe C–Br bond fission mainly in the anti conformer. The lack of C–Br bond fission in the *gauche* conformer results because of a large energetic splitting between adiabats at the barrier to C–C bond fission in *gauche* bromoacetone. As a result of this large splitting, C–C bond fission completely dominates C–Br bond fission in *gauche* bromoacetone. In antibromoacetone, however, the splitting between adiabats at the barrier to C–C bond fission is 0 cm^{-1} since the adiabats meet at a conical intersection. Consequently, in antibromoacetone C–Br bond fission competes effectively with C–C bond fission.

ACKNOWLEDGMENTS

This work was supported by the National Science Foundation under Grants number CHE-9007769 and CHE-8857209. M.M.F. was supported by a Summer Faculty Research Fellowship, a supplement to our grant (#22218-AC6) from the donors of The Petroleum Research Fund, administered by the ACS, and by the Rosalyn R. Schwartz Lectureship. P.W.K. was supported in part by a Department of Education GANN fellowship. G.C.G.W. was supported by a Clare Boothe Luce Graduate Fellowship. L.J.B. gratefully acknowledges the support of a Camille and Henry Dreyfus Foundation Teacher–Scholar Award and an Alfred P. Sloan Research Fellowship. We also thank J. Stevens, Professor J. Michl, Professor A. Kuki, and Professor K. Jordan for helpful discussions on this work.

[1] The development of statistical transition state theories is reviewed by K. J. Laidler and M. C. King, J. Phys. Chem. **87**, 2657 (1983).
[2] The current status of statistical transition state theory is reviewed by D. G. Truhlar, W. L. Hase, and J. T. Hynes, J. Phys. Chem. **87**, 2664 (1983).
[3] P. J. Robinson and K. A. Holbrook, *Unimolecular Reactions* (Wiley-Interscience, London, 1972).
[4] See, for example, L. J. Butler, R. J. Buss, R. J. Brudzynski, and Y. T. Lee, J. Phys. Chem. **87**, 5106 (1983).

[5] See, for example, D. Krajnovich, F. Huisken, Z. Zhang, Y. R. Shen, and Y. T. Lee, J. Chem. Phys. **77**, 5977 (1982).
[6] M. D. Person, P. W. Kash, S. A. Schofield, and L. J. Butler, J. Chem. Phys. **95**, 3843 (1991).
[7] M. D. Person, P. W. Kash, and L. J. Butler, J. Chem. Phys. **97**, 355 (1992).
[8] The universal detector was introduced by Y. T. Lee, J. D. McDonald, P. R. LeBreton, and D. R. Herschbach, Rev. Sci. Instrum. **40**, 1402 (1969).
[9] For details, see M. D. Person, Ph.D. thesis, Department of Chemistry, University of Chicago, 1991.
[10] GAUSSIAN 92, Revision C, M. J. Frisch, G. W. Trucks, M. Head-Gordon, P. M. W. Gill, M. W. Wong, J. B. Foresman, B. G. Johnson, H. B. Schlegel, M. A. Robb, E. S. Replogle, R. Gomperts, J. L. Andres, K. Raghavachari, J. S. Binkley, C. Gonzalez, R. L. Martin, D. J. Fox, D. J. Defrees, J. Baker, J. J. P. Stewart, and J. A. Pople (Gaussian, Inc., Pittsburgh, 1992).
[11] M. D. Person, P. W. Kash, and L. J. Butler, J. Phys. Chem. **96**, 2021 (1992).
[12] P. W. Kash, G. C. G. Waschewsky, R. E. Morss, L. J. Butler, and M. M. Francl, J. Chem. Phys. (submitted).
[13] R. N. Zare, Mol. Photochem. **4**, 1 (1972).
[14] L. J. Butler, E. J. Hintsa, S. F. Shane, and Y. T. Lee, J. Chem. Phys. **86**, 2051 (1987).
[15] R. Stolevik and P. Bakken, J. Mol. Struc. **159**, 311 (1987).
[16] The expression $\beta=2P_2(\cos\alpha)$ is given in G. E. Busch and K. R. Wilson, J. Chem. Phys. **56**, 3638 (1972); S. C. Yang and R. Bersohn, *ibid.* **61**, 4400 (1974).
[17] D. J. Krajnovich, Ph.D. thesis, Appendix B, University of California, Berkeley, 1983.
[18] We estimate the ionization cross section using the empirical relationship obtained in R. E. Center and A. Mandl, J. Chem. Phys. **57**, 4104 (1972), $\sigma_{\text{ion}}(10^{-16}\ \text{Å}^2)=36(\alpha^{1/2})-18$. The atomic polarizabilities, α, of 3.05 and 2.18 Å^3 for Br and Cl are given in T. M. Miller and B. Bederson, Adv. At. Mol. Phys. **13**, 1 (1977).
[19] Our forward convolution programs for the center-of-mass to laboratory frame transformations were adapted from the CMLAB programs written by the Y. T. Lee group.
[20] J. I. Steinfeld, J. S. Francisco, and W. L. Hase, *Chemical Kinetics and Dynamics* (Prentice–Hall, Englewood Cliffs, 1989), p. 314.
[21] See, for example, A. McIlroy and D. J. Nesbitt, J. Chem. Phys. **92**, 2229 (1990).
[22] J. Michl and V. Bonačić-Koutecký, *Electronic Aspects of Organic Photochemistry* (Wiley, New York, 1990), p. 276.
[23] R. B. Woodward and R. Hoffmann, *The Conservation of Orbital Symmetry* (Chemie, Weingeim/Bergstrasse, 1970).
[24] This expression may be derived from Eq. (9) in D. M. Silver, J. Am. Chem. Soc. **96**, 5959 (1974). The Silver paper considers the energy lowering, ΔE, of the barrier from the diabatic crossing. ΔE should be equivalent to V_{12}, but Silver's expression for ΔE includes several typos.
[25] G. L. Closs, P. Piotrowiak, J. M. MacInnis, and G. R. Fleming, J. Am. Chem. Soc. **110**, 2652 (1988).
[26] S. Levy, M. B. Rubin, and S. Speiser, J. Photochem. Photobiol. A Chem. **66**, 159 (1992).